VII Jornades IdISBa

PÒSTERS DE L'ÀREA:

Àrea Transversal de Ciència i Tecnologia en Salut

Institut d'Investigació Sanitària Illes Balears

IdISBa

Deep Learning-based Object Detection for a Quality Control Application in the Sterilization Unit of a Hospital

Kai Yao, **Alberto Ortiz & Francisco Bonnin-Pascual**
Department of Mathematics and Computer Science
University of the Balearic Islands

Abstract: In this work, we describe an object recognition solution aiming at detecting the presence of quality control elements in surgery toolboxes handled by the *Sterilization Unit* of a hospital. Our solution actually consists in a ***two-stage*** *arbitrarily-oriented object detection method* making use of indirect regression of oriented bounding boxes parameters. The paper describes the design process and reports on the results obtained up to date.

Quality Control Elements From left to right, we show the four kinds of elements to be detected: the *label* used to track a box of tools, the yellowish *seal*, the *paper tape* which changes to the stripped appearance when the box has been inside the autoclave, and an *internal filter* which is placed inside some boxes and creates the white-dotted texture that can be observed (instead of black-dotted).

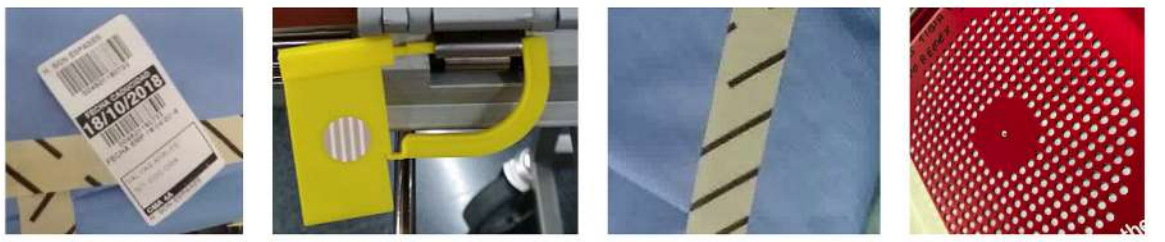

Detector Overview

First Stage: Unoriented Bounding Boxes Detection

1. Ground Truth Definition

For the first stage, we define two training datasets due to the elongated shape of the paper tape: *Dataset A* (left) associates one box for every object while *Dataset B* (right) associates several boxes per object to cover the paper tape in a better way.

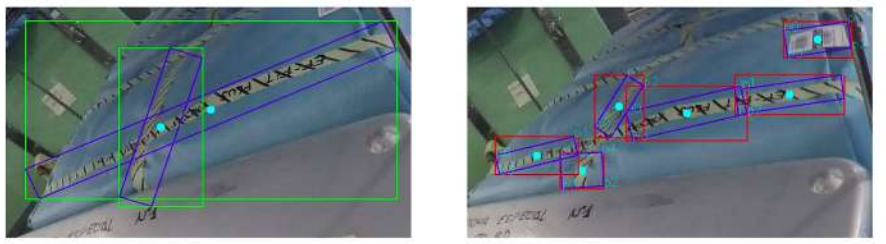

2. K-means Clustering for Default Boxes Selection

In order to obtain high quality default boxes, we run the well-known K-means algorithm over the bounding boxes defined in the ground truth, using boxes width and height as the clustering features. The distance between a sample box b_i and the cluster centroid c_j is defined as:

$$d(b_i, c_j) = 1 - \text{IoU}(b_i, c_j) = 1 - \frac{o(b_i, c_j)}{a(b_i) + a(c_j) - o(b_i, c_j)}$$

where $o(\cdot, \cdot)$ denotes area overlap and $a(\cdot)$ denotes area.

AVERAGE IOU (AVIOU) OF DEFAULT BOXES VS SELECTION APPROACH

Dataset	Approach	# def. boxes	AvIoU (%)
A	Hand-Picked	4	35.39
	Hand-Picked	5	38.53
	Hand-Picked	6	51.81
	Hand-Picked	10	60.24
	Clustering	4	62.81
	Clustering	5	67.75
	Clustering	6	68.90 ←
B	Hand-Picked	4	30.03
	Hand-Picked	5	32.09
	Hand-Picked	6	51.55
	Hand-Picked	10	61.36
	Clustering	4	65.64
	Clustering	5	66.46
	Clustering	6	67.25 ←

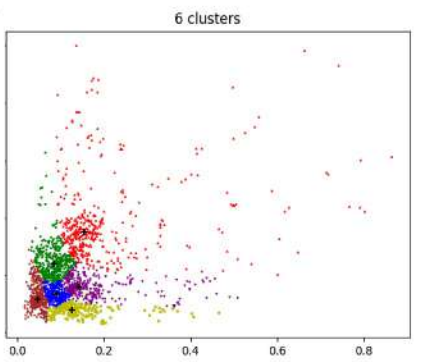

3. Unoriented Bounding Boxes Regression

We use the *Single Shot Multibox Detector* (SSD) to predict bounding boxes containing the objects of interest. SSD provides category scores and box coordinates from predicted box offsets for a fixed set of default bounding boxes using a set of convolutional filters applied to feature maps. The overall loss function is a weighted sum of the localization loss L_{loc} and the category loss L_{conf}.

$$L(x, c, l, g) = \frac{1}{N}\left(L_{\text{conf}}(x, c) + \alpha L_{\text{loc}}(x, l, g)\right)$$

where x_{ij}^p are the indicator functions that match predicted boxes to ground truth boxes, and c, l, g represent the predicted category, the box coordinates and the ground truth box. α balances the impact of the category and the localization losses.

Second Stage: Oriented Bounding Boxes Detection

1. Approach and Ground Truth Definition

The second and final stage, i.e. regression of oriented bounding boxes parameters, makes use of a specifically designed lightweight CNN for improved performance.

For training, we define the ground truth parameters by the intersects d_1 and d_2 of the upper side of the rotated rectangle with the sides of the unrotated rectangle.

Optionally, we also add parameter h to choose one of the two possible oriented rectangles. Besides, we also define a clockwise order onto the four corners of the rotated box.

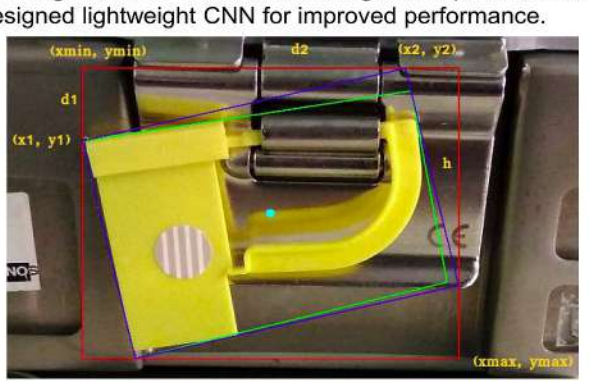

2. Network Architecture

The network is inspired by the LeNet CNN. Further, we increase the input size from 28x28 pixels to 63x63 pixels and, in order to speed up network convergence, we use batch-normalization layers after convolutional layers. A final sigmoid layer is added to normalize the output values.

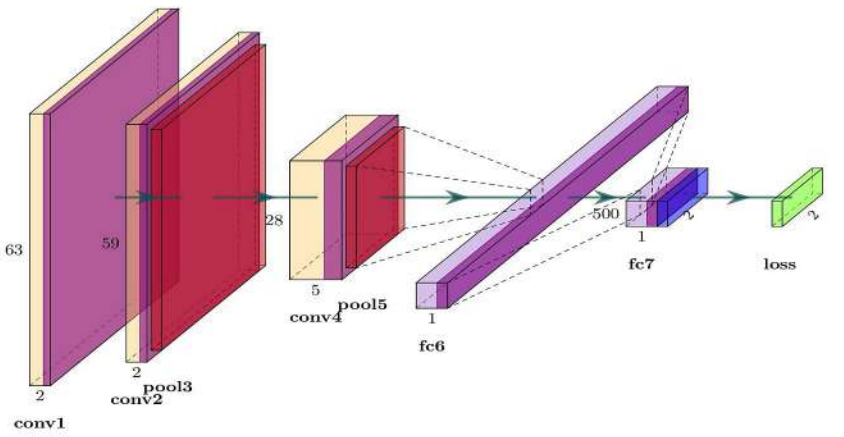

3. Oriented Bounding Boxes Regression

The final loss function is implemented by means of an Euclidean loss layer as follows:

$$L(d, g) = \frac{1}{2N}\sum_{i \in N}(\|d_1^i - g_1^i\|_2^2 + \|d_2^i - g_2^i\|_2^2 + \|d_h^i - g_h^i\|_2^2)$$

where d denotes the predicted intercepts and height, g denotes the ground truth, and N is the size of the minibatch.

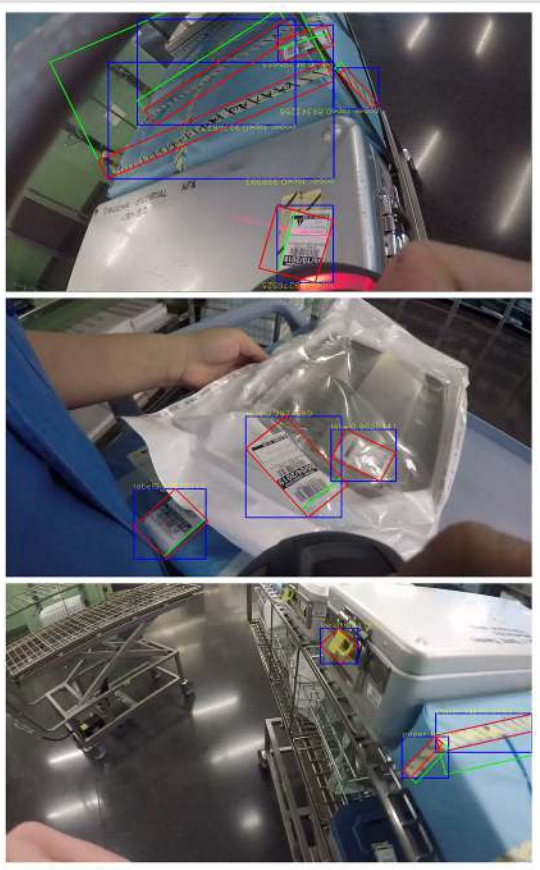

Experimental Results

Standard *Recall* (R), *Precision* (P), *Mean Average Precision* (mAP) and *Average Intersection-over-Union* (AvIoU) performance metric values have been calculated for quantitative evaluation and comparison. In this assessment, true positives have been defined in accordance to a threshold of 0.5 for the IoU between ground truth and predicted bounding boxes.

As expected, the predictions corresponding to the training dataset B are of better quality than those corresponding to dataset A. Hence, below we show results for the former training, highlighting the best results in red (with regard to dataset A results).

PERFORMANCE RESULTS FOR UNORIENTED OBJECT DETECTION

Datas.	#	Class	R	P	mAP	AvIoU
B	4	Label	0.9637	0.9871	0.9627	0.8781
		Seal	0.9693	0.9813	0.9687	0.8609
		Paper Tape	0.8742	0.9704	0.8804	0.8406
		Intl. Filter	0.8783	1.0000	0.8783	0.8928
	Average		0.9214	0.9847	0.9225	0.8681
	5	Label	0.9306	0.9870	0.9298	0.8460
		Seal	0.8775	0.9772	0.8775	0.8112
		Paper Tape	0.8948	0.9383	0.8893	0.7699
		Intl. Filter	0.9047	0.9500	0.8714	0.8120
	Average		0.9019	0.9631	0.8522	0.8098
	6	Label	0.9721	0.9872	0.9729	0.8861
		Seal	0.9631	0.9751	0.9618	0.8599
		Paper Tape	0.8831	0.9742	0.8879	0.8486
		Intl. Filter	0.9054	1.0000	0.9054	0.8927
	Average		0.9309	0.9841	0.9320	0.8719

The table below shows results of oriented object detection, using dataset B and 6 clusters during training, accordingly to the unoriented bounding boxes detection results.

In the comparison, we consider the loss function for both 2 term-, i.e. (d_1, d_2), and 3 term- parameterizations, i.e. (d_1, d_2, h). Additionally, we report results for AlexNet as a baseline (properly tuned for the detection problem at hand).

PERFORMANCE RESULTS FOR ORIENTED OBJECTS DETECTION

Method	Class	R	P	mAP	AvIoU
2 param.	Label	0.8204	0.8445	0.7633	0.6649
	Seal	0.7346	0.8000	0.6254	0.6451
	Paper tape	0.5257	0.6071	0.4080	0.5517
	Intl. Filter	0.5454	0.6667	0.3916	0.5142
	Average	0.6566	0.7295	0.5471	0.5940
3 param.	Label	0.6571	0.6764	0.5505	0.5718
	Seal	0.6326	0.6889	0.4810	0.5480
	Paper tape	0.2422	0.2797	0.1254	0.3898
	Intl. Filter	0.3809	0.4210	0.2208	0.3888
	Average	0.4782	0.5165	0.3444	0.4746
AlexNet	Label	0.5387	0.5546	0.3752	0.5107
	Seal	0.6530	0.7111	0.5064	0.5578
	Paper tape	0.1695	0.1803	0.1063	0.3624
	Intl. Filter	0.5238	0.5789	0.4556	0.5289
	Average	0.4713	0.5062	0.3684	0.4900

*** PC fitted with an NVIDIA GeForce GTX 1080 GPU, a 2.9GHz 12-core CPU with 32 Gb RAM and Ubuntu 64-bit

This work is partially supported by projects BUGWRIGHT2 (EU-H2020, GA 871260), ROBINS (EU-H2020, GA 779776), PGC2018-095709-B-C21 (MCIU/AEI/FEDER, UE), and PROCOE/4/2017 (Govern Balear, 50% P.O. FEDER 2014-2020 Illes Balears).
The European Union is not liable for any use that may be made of the information contained in this publication.

Modelo para la gestion de solicitudes de resonancia magnética: Aplicación a la programación musculoesquelética del Servicio de Radiodiagnóstico del Hospital Universitario de Son Espases

Irene García Mosquera[1,3], Reda Britel[2], Lorenzo Muntaner[2], Teresa Anglada[1], Joan Palmer Sancho[2], Olga Bonnin Arnas[2]

Universitat de les Illes Balears — Grup de recerca de Biologia Computacional i Bioinformàtica

Son Espases hospital universitari

Institut d'Investigació Sanitària Illes Balears

Introducción

- El tiempo de espera es uno de los factores que el usuario identifica más claramente con la calidad del servicio sanitario y constituye uno de los aspectos a mejorar https://www.ibsalut.es/es/info-ciudadania/listas-de-espera .
- La demanda de RM crece cada día por su importancia para el diagnóstico de lesiones y enfermedades. Adicionalmente, la crisis sanitaria generada por el COVID-19, ha saturado aún más la capacidad de afrontar el tiempo de espera estructural de citas de patologías no directamente vinculadas con la pandemia.
- Los costos derivados de la asignación ineficiente de citas son elevados y la capacidad de los servicios está limitada en recursos de personal y estructura.
- Recientemente la SERAM ha publicado una guía de priorización que permite organizar las citaciones de las pruebas de pacientes con criterios clínicos, teniendo una mirada sensible en beneficio de los pacientes más vulnerables https://www.seram.es/index.php/seram-rss/1495-nuevo-documento-citacion-pruebas-radiologia-en-la-era-post-covid19

Modelo propuesto

$$Indice = 0,7\ Prioridad + 0,2\ CEX + 0,1\ Peticion$$

El índice pone la mayor ponderación en las normas de la SERAM porque estos criterios sugieren una respuesta temporal adecuada y objetiva en cada caso. En segundo lugar, el índice pondera el número de días que faltan para la cita de consulta externa (fecha en que se supone que debe estar lista la RM) y, por último, toma en cuenta el número de días desde la solicitud.

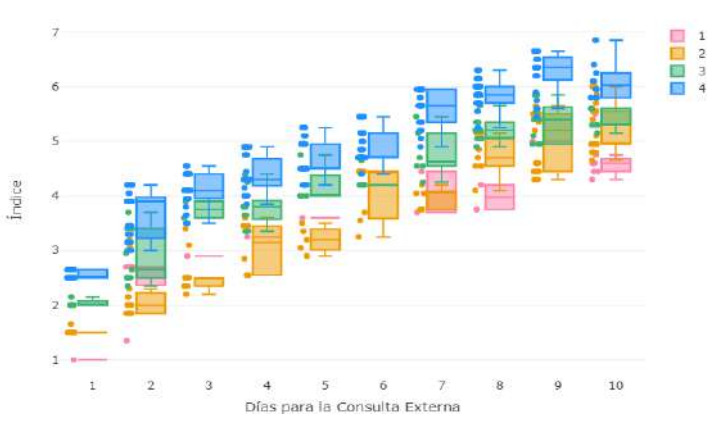

El total de solicitudes corresponde a 739 tiempos de citas (huecos). Con 28 días de 12 huecos por la mañana y 15 por la tarde se podrían atender todas las solicitudes.

Pacientes a citar en la mañana

ID	Prioridad	Huecos	Dias_cex_cat	Dias_cex	Dias_pet_cat	Dias_pet	Indice
Paciente 9	1	2	1	-195	1	374	1.00
Paciente 14	1	2	2	4	1	360	1.35
Paciente 149	2	2	1	-319	1	408	1.50
Paciente 165	2	2	1	-240	1	419	1.50
Paciente 166	2	1	1	-212	1	391	1.50
Paciente 172	2	2	1	-450	1	509	1.50

Objetivos

- Identificar las distorsiones o los aumentos del tiempo de espera.
- Desarrollar un modelo que incorpore tanto los criterios clínicos recogidos en el documento publicado por la Sociedad Española de Radiología Médica (SERAM) como los factores estructurales del Servicio de Radiología de Son Espases.
- Organizar las citaciones de los pacientes más vulnerables y cumplir las garantías de demora estructural contempladas en Decreto 31/2018, BOIB.

Resultados

Contrastamos el índice con la citación real de una muestra aleatoria de 33 solicitudes atendidas entre el 21/05 y el 02/10 de 2020

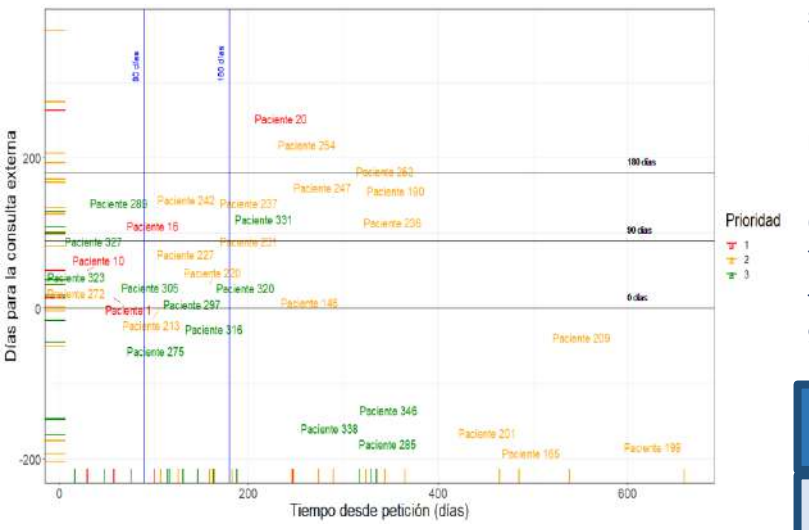

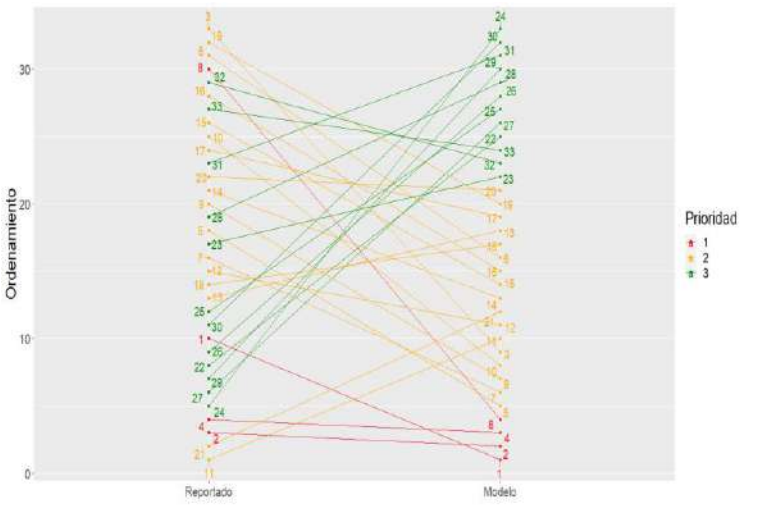

El modelo ordena las solicitudes para favorecer el abordaje de dolencias clínicamente prioritarias, a la par que permite la gestión eficiente del Decreto 31/2018 BOIB de garantía de demoras de la lista de espera estructural.

Agradecimientos

Este trabajo ha sido apoyado por el Ministerio de Ciencias, Innovación y Universidades Español y por el Fondo para el desarrollo Europeo a través del proyecto: **PGC2018-096956-B-C43 (FEDER/MICINN/AEI)**

Materiales y Métodos

Trabajamos con una base de datos anonimizada del buzón de solicitudes de resonancia magnética (RM) musculoesquelética constituida por 561 solicitudes de RM y 10 variables registradas:

- ID: identificador numérico del paciente (simula Nº historia).
- **Prioridad:** indica prioridad de la solicitud. Un número grande indica una solicitud ordinaria, de acuerdo a los criterios de la SERAM.
- Resonancia: equipo de resonancia al cual puede ser asignado el paciente. 77% de las solicitudes pueden ir a "1/3/4" cualquiera de los 3 equipos.
- Turno: Mañana, Tarde y Fin de semana. No resultó significativa. Los casos difíciles suelen ser asignados por la mañana y los que no requieren presencia del médico en fin de semana.
- Tiempo de cita: cuántos intervalos de 20 minutos (huecos) se necesitarán para hacer la RM. 69% de las solicitudes requerían 1 hueco.
- COTMES: indicador de si el caso ha sido estudiado por el Comité Musculoesquelético del HUSE. 15% de las solicitudes han pasado por COTMES.

Días de petición: días transcurridos desde la fecha de registro.

Días CEX: días que faltan para la consulta externa del paciente a la cual debe llevar la RM.

Objetivo de visita: diagnóstico (77%) o seguimiento, se tomará en cuenta para futuros modelos.

Tipo de cita: zona del cuerpo donde se realizará la RM. 96% son extremidades.

Conclusiones y trabajo futuro

- Este orden de citación dará origen a consultas con alta resolución, la RM solicitada estará lista el día de la consulta.
- La implementación facilitaría la tarea del personal administrativo. Permitiría diversificar su actividad para que colabore, en la recogida de indicadores de calidad.
- Estamos desarrollando un modelo de teoría de colas que tome en cuenta el número de equipos de resonancia y optimice el tiempo de espera medio de cada paciente. Referencia: An adaptive priority policy for radiotherapy scheduling. S. Li. Flexible Services and Manufacturing Journal Vol.32, pp154–180(2020).

Información de contacto

Irene García — irene.garcia@uib.es

Reda Britel — reda.britel@gmail.com

Effect of titanium functionalization with platelet-derived extracellular vesicles on biocompatibility and mesenchymal stem cell differentiation

M. Antich-Rosselló; M.A. Forteza-Genestra; A. Gayà; J. Calvo; M. Monjo; J.M. Ramis

Background and Aim

Titanium (Ti) implants are widely used in regenerative medicine with several applications such as orthopedic and dental implants. Ti surfaces are directly exposed to the patient's tissues. Thus, to improve osteointegration and tissue response their modification is being explored. One strategy is their functionalization with active biocomponents. Some studies suggest that platelet concentrates, like Platelet Lysate (PL) can enhance titanium osteointegration. However, these strategies present high variability in the obtained results, limiting their regular clinical use. Here, we propose the use of platelet-derived Extracellular Vesicles (EVs) as functional coating for Ti implants.

Materials & Methods

1. EVs isolation

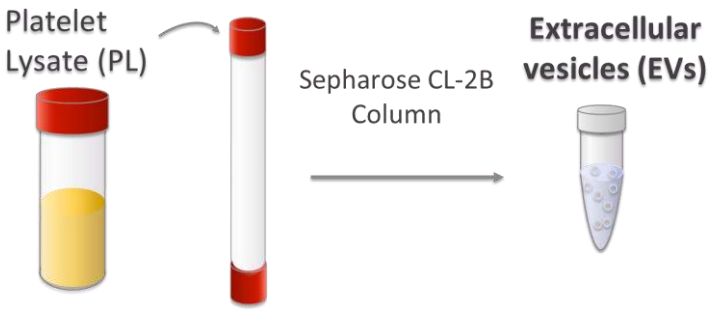

2.Ti functionalization

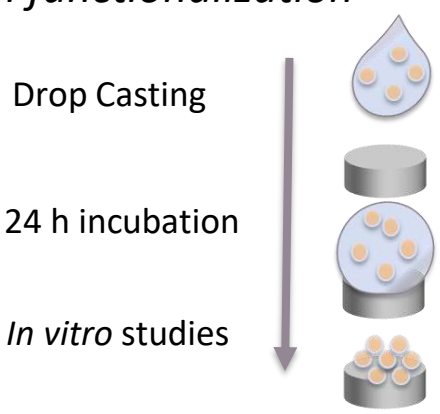

3. In vitro *studies*

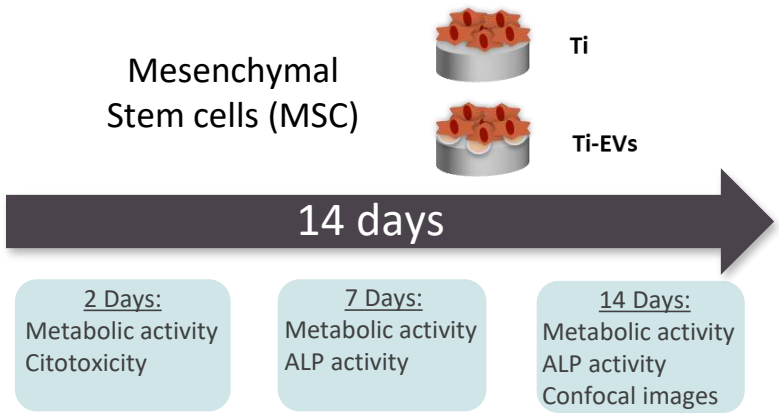

Results

1. Biocompatibility

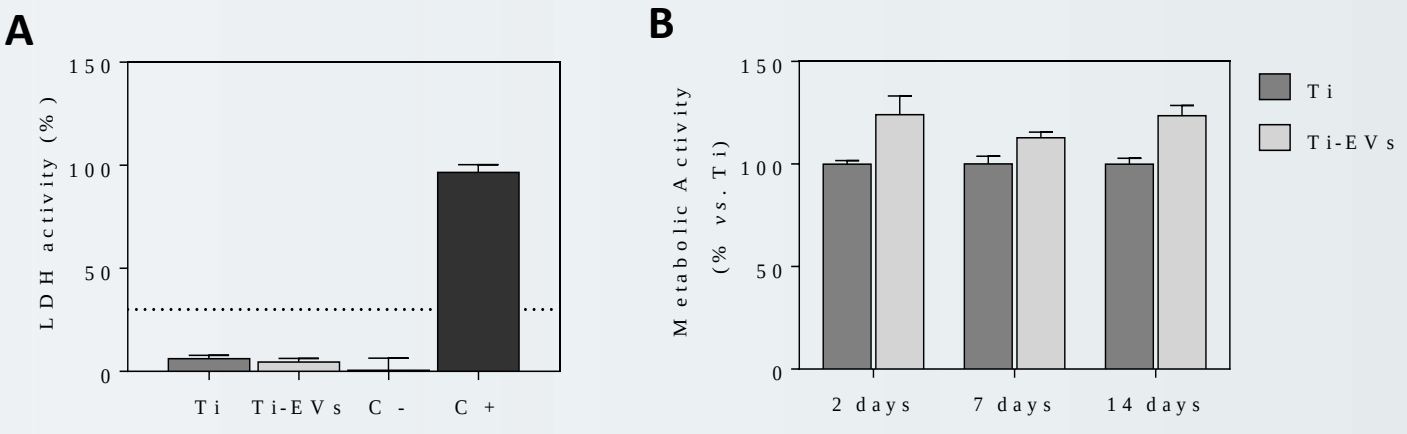

Figure 1: Surface biocompatibility on Mesenchymal Stem Cells (MSC). **A)** Cytotoxicity of cells cultured on the titanium surfaces (Ti) and the Extracellular Vesicles functionalized Ti surfaces (Ti-EVs), measured as LDH activity; cells cultured onto tissue culture plastic are considered (C -) and set to 0 %, while MSCs cultured onto plastic and treated with Triton 100X 1% are considered (C +) and set to 100 %. **B)** Metabolic Activity of MSC cultured on the Ti and the Ti-EVs surfaces at 2, 7 and 14 days. Ti group was set at 100 % for each day. **C)** Cell morphology after 14 days of cell culture on Ti surface (left) and Ti-EVs surface (right). The images represent MSCs stained with Phalloidin-FITC (green) and DAPI (blue).

2. Bone differentiation

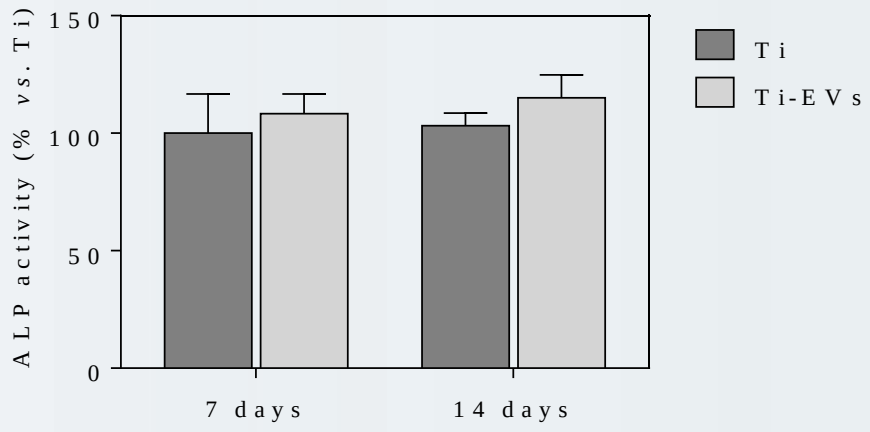

Figure 2: Mesenchymal Stem Cell (MSC) differentiation. Bone differentiation of MSC cultured on Ti and Ti-EVs surfaces at 7 and 14 days measured by Alkaline Phosphatase (ALP) activity. ALP activity of Ti group was set at 100 % for each day.

Conclusions

- Ti surfaces functionalized with PL-derived EVs by drop casting show improved biocompatibility.
- PL-derived EVs present an osteogenic capability, improving Ti surfaces functionality.
- Further *in vivo* studies are required in order to confirm the value of our *in vitro* findings.

Acknowledgements: *This work was supported by the Instituto de Salud Carlos III (contract to J.M.R MS16/00124 and M.A.F.G. CP16/00124), the Vicepresidència I Conselleria d'Innovació, Recerca I Turisme del Govern de les Illes Balears (contract to M.A.R.; FPI/2046/2017) and PROGRAMA JUNIOR del proyecto TALENT PLUS, contruyendo VALOR, generando SALUD (contract to M.A.F.G.) . The authors thank G. Ramis (UIB) for his technical contribution with Confocal microscopy.*

Platelet lysate-derived extracellular vesicles improve regeneration of osteoarthritic cartilage explants

Maria Antònia Forteza-Genestra; Miquel Antich-Rosselló; Antoni Gayà; Javier Calvo; Marta Monjo; Joana M. Ramis

IdISBa

Universitat de les Illes Balears

Background and Aim

Osteoarthritis (OA)

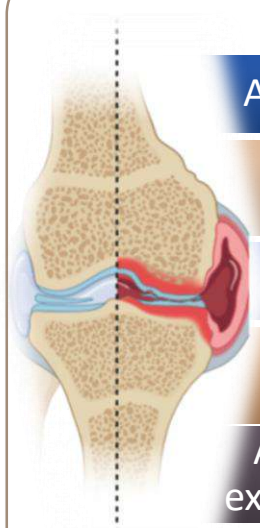

- Articular degenerative process.
- Irreversible inflammation and destruction of extracellular matrix (ECM) of articular cartilage.
- Loss of glycosaminoglycan (GAG).
- Minimal-invasive surgical method: injection of platelet rich plasma (PRP).
- Alternative: Platelet lysate (PL) derived extracellular vesicles (EVs)

Advantages of EV use in regenerative medicine

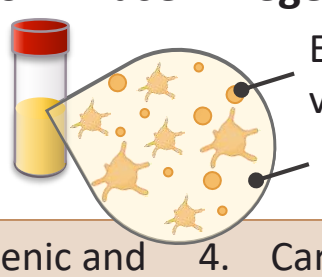

1. Less tumorigenic and immunogenic.
2. Can be sterilized.
3. Easy storage and manipulation.
4. Cargo protection from *in vivo* degradation.
5. Easy characterization and standardization.

Our **aim** was to evaluate the effectiveness of PL-derived EVs for the recovery of human cartilage explants with induced OA.

Materials and Methods

Cartilage explants from human cartilages

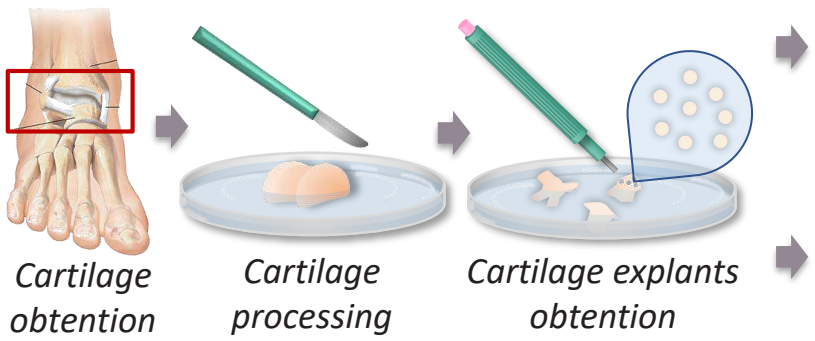

In vitro tissue culture

DMEM-F12 + **inflammatory condition**:
0.1 µg/µl Oncostatin S
0.01 µg/µl TNFα

DMEM-F12 + **inflammatory condition** + **EV treatments**:
PL → 5 µg protein
PL-EVs Low Dose (LD) → $1x10^8$ particles
PL-EVs High Dose (HD) → $1x10^9$ particles

Analysis

Characterization at day 1, 7 & 14:
COL2A1 | *ACAN*

EV treatments for 14 days:
GAG quantification
Sirius Red staining

Results

Characterization of normal and inflamed explants

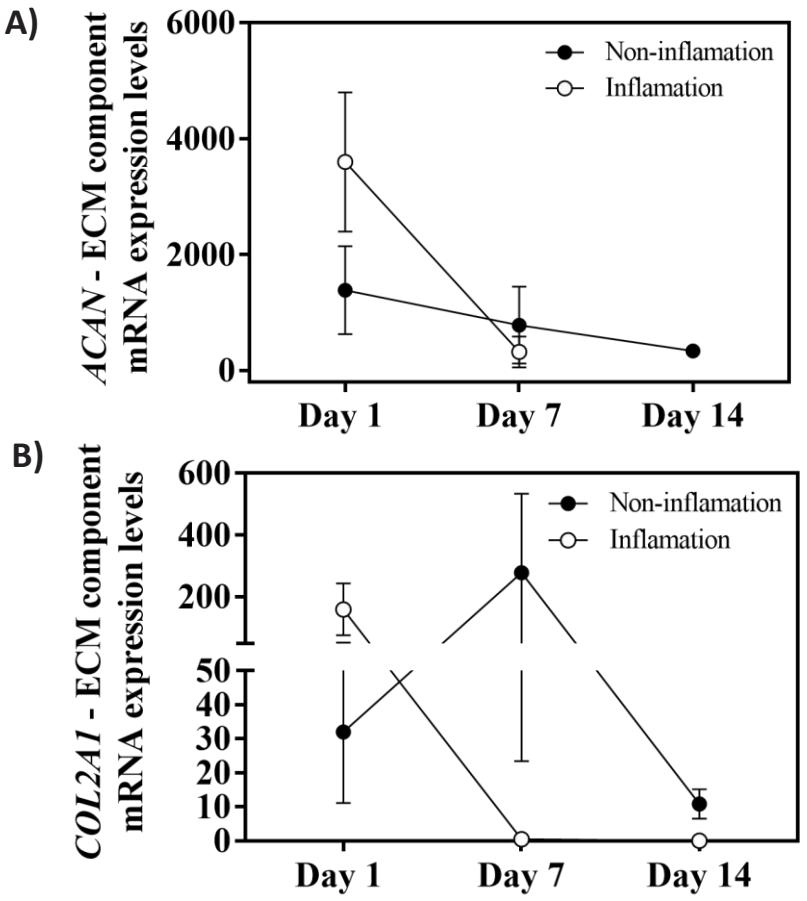

Figure 1. ACAN and COL2A1 gene expression relative levels. ECM components *ACAN* (A) and *COL2A1* (B) relative mRNA expression levels at day 1, 7 and 14 with or without inflammation (n=3).

EV treatments on cartilage explants for 14 days

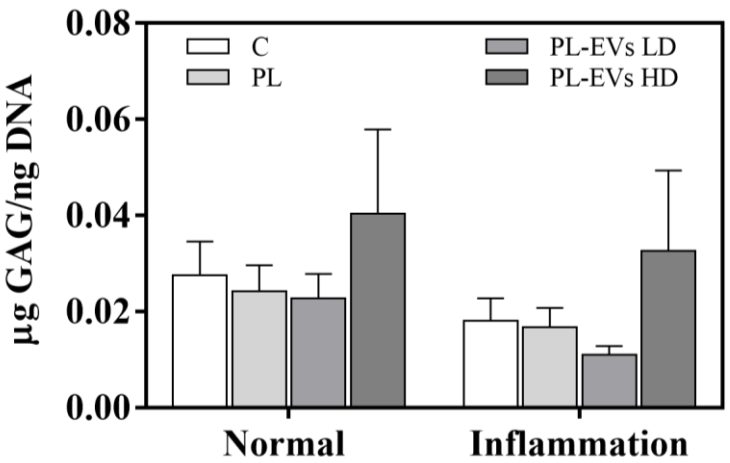

Figure 2. GAG quantification after 14 days of EV treatments. Results normalized by DNA content. Bar plot represent mean values with SEM (n=13 -C- ; n=16 -PL and PL-EVs LD-; n=6 -PL-EVs HD-). Results were statistically compared by Kruskal-Wallis.

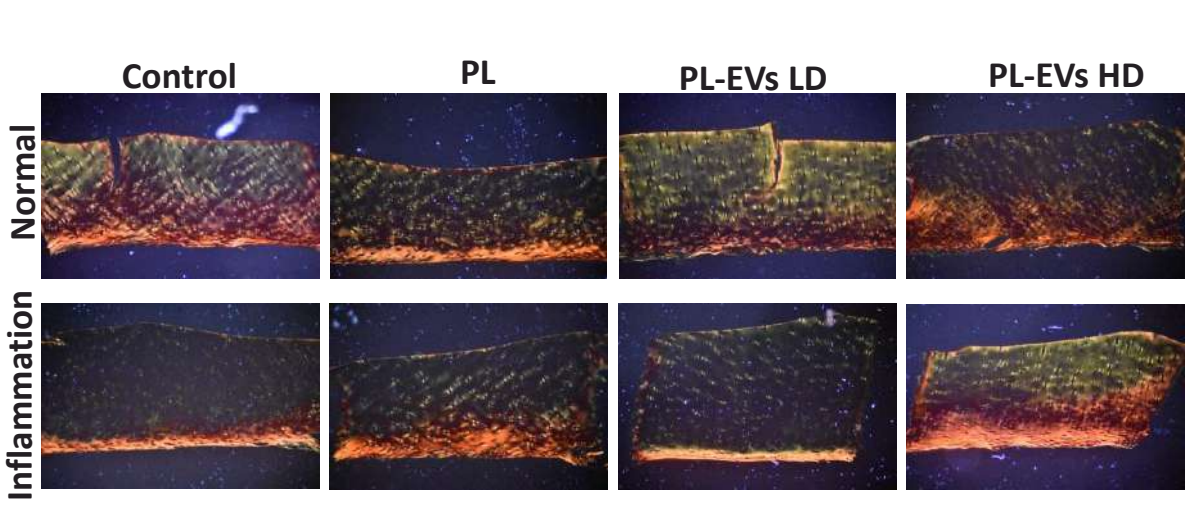

Figure 3. Sirius red staining after 14 days of EV treatments. Six micrometers tissue sections were stained and images taken at 100x under polarized light. Bright yellow or orange = larger collagen fibers; Green = thin/reticular fibers.

In conclusion, although more samples need to be evaluated, the results obtained so far indicate that high dose of PL-derived EVs improve regeneration of osteoarthritic cartilage explants.

Acknowledgements: *This work was supported by the Instituto de Salud Carlos III, Ministerio de Economía y Competividad, co-funded by the ESF European Social Fund and the ERDF European Regional Development Fund (MS16/00124; CP16/00124), the Vicepresidència I Conselleria d'Innovació, Recerca I Turisme del Govern de les Illes Balears (contract to M.A.R.; FPI/2046/2017) and PROGRAMA JUNIOR del proyecto TALENT PLUS, construyendo VALOR, generando SALUD (contract to M.A.F.G.) .*

TERCIT webpage: *https://tercit.wordpress.com/* ***Contact e-mail:*** *maria.forteza@ssib.es or joana.ramis@uib.es*

MASK3D4ALL: Projecte per l'Autofabricació 3D de mascaretes amb filtres Bioactius contra la COVID19

B. Alorda-Ladaria, J. Reyes, Y. González, P. Roca

Universitat de les Illes Balears

Institut d'Investigació Sanitària Illes Balears
IdISBa

Problemàtica i objectius del treball

Com garantir disposar d'EPIs suficients en situacions de Pandèmia global?

Com reciclar l'estoc de material EPI homologat per mantenir nivell de protecció davant pandèmies respiratòries?

Com incorporar capacitats virucides als elements filtrants de les mascaretes?

Hipòtesi 1: Una tela filtrant amb solució salina pot tenir capacitat virucida

Hipòtesi 2: La fabricació aditiva 3D pot contribuir a proveir d'EPIs vàlides pel reciclatge i la protecció

Objectiu: Definir un protocol d'autoprotecció vàlid tant per punts calents sanitaris com també per la resta de la població

Avaluar tant els materials de fabricació nacional, les eines de producció Km 0 i la incorporació de solucions salines als elements filtrants

Metodologia i Activitats

Experiments d'observació: comprovar la quantitat de NaCL deposidad a la tela

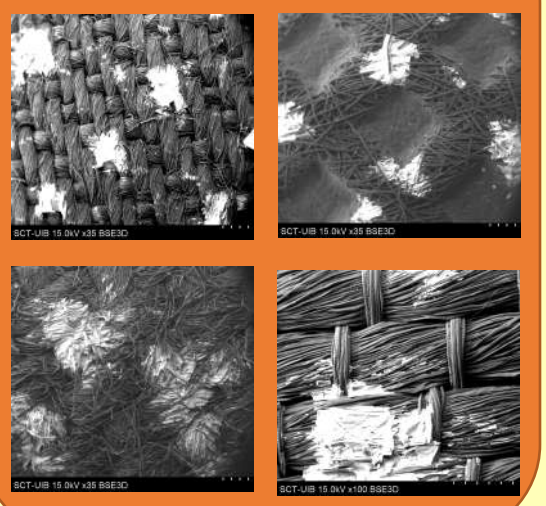

Avaluació de teles de proveïdors locals:

- Cotó
- Tela no teixit
- Lynocell
- Tencel
- Poliestirer
- Seda natural

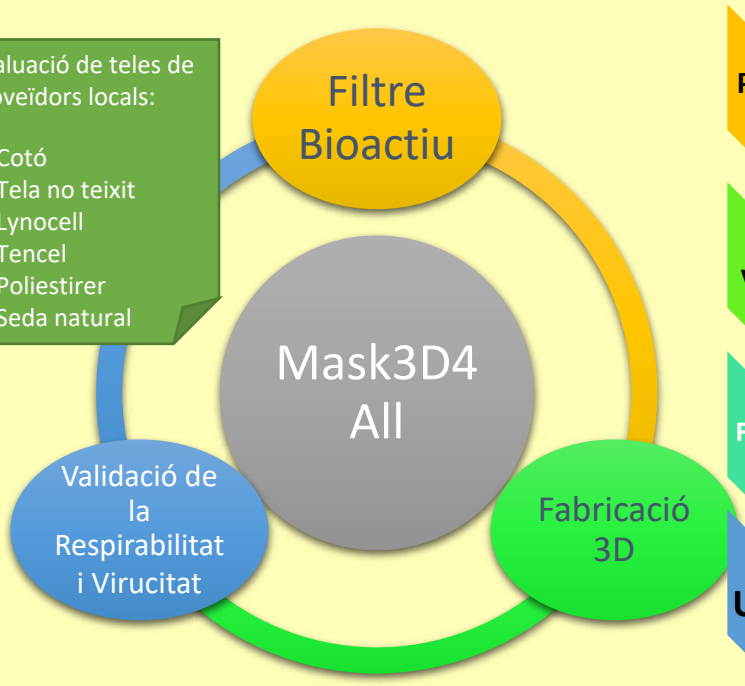

Preparar filtres
- Selecció de les teles disponibles en local que poden tenir un comportament adequat com a elements filtrants
- Desenvolupament de la metodologia per dipositar solució salina i crear filtre bioactiu

Validació
- Validació de la dispersió sobre la tela amb microscopia electrònica i òptica
- Validació de la respirabilitat segons norma UNE-EN 14683:2019
- Validació de la virucitat amb virus SARS

Fabricació 3D
- Fabricació amb impressores de gama mitja
- Fabricació amb impressores de gama industrial
- Exploració de nous dissenys oberts amb protecció ocular

Usuaris
- Validació de la usabilitat dels prototips
- Comportament davant els processos d'esterilització
- Personalització del disseny 3D

Resultats del projecte en curs

eISSN 2255-0569

ORIGINAL

Proyecto para la autofabricación de mascarillas con filtros bioactivos y tecnología de impresión 3D para la lucha contra la COVID en Baleares

Project for the self-manufacturing of maskswith bioactive filters and 3D printing technology for the fight against COVID in the Balearic Islands

Bartomeu Alorda[1], José Reyes[2], Yolanda González Cid[1], Pilar Roca[2]

1. Grupo de eHealth y Telemedicina multidisciplinar mediante sistemas inteligentes ciberfísicos (IDISBA).
2. Grupo multidisciplinar de oncología traslacional (GMOT) del Instituto de Investigación Sanitaria de las Islas Baleares (IDISBA).

Correspondencia
José Reyes
Instituto de Investigación Sanitaria de las Islas Baleares (IDISBA)
Hospital Universitari Son Espases
Ctra. de Valldemossa, 79 - 07120 Palma de Mallorca
E-mail: jose.reyes@hcin.es

Recibido: 14 -IX - 2020
Aceptado: 23 - X - 2020

doi: 10.3306/MEDICINABALEAR.35.04.78

Resumen

La pandemia creada por la COVID19 está revisando todos los protocolos que hasta ahora se venían poniendo en marcha en la sanidad pública. Uno de ellos es el abastecimiento de equipos de protección individual de los centros sanitarios y hospitales que se vio comprometido durante los primeros meses de una pandemia con afectación global. Depender del suministro exterior de equipos de protección personales no contribuye a una rápida respuesta de protección. El proyecto Mask3D4All pretende definir un proceso de autoproducción de mascarillas faciales con capacidades virucidas mediante la evaluación de técnicas de fabricación 3D y la incorporación de soluciones salinas en los elementos filtrantes. Los resultados de este proyecto permitirán definir un protocolo de autoprotección no solo válido para los puntos calientes sanitarios, sino también para la protección del resto de la población y centros sociales al basar los estudios en materiales de fabricación nacional para afrontar un posible cierre del comercio entre países.

Palabras clave: COVID-19, SARS-COV-2, EPI (Equipo Protección Individual), Mascarilla Respiratoria, Impresión 3D.

Amb una metodologia basada en una solució salina saturada s'han aconseguit dipòsits entre el 3,4 i 18,9 mg/cm^2

FILTRE BIOACTIU

El test de Respirabilitat del filtre Salí indica una pressió diferencial inferior a 60 Pa/cm^2 segons normativa UNE-EN 14683:2019

Estam a l'espera dels resultats de virucitat!!

Dissenys de Fabricació 3D

S'estima que l'ús de mascaretes de fabricació 3D permetria una optimització de fins a 5 vegades el material EPI homologat disponible.

Per exemple: cada mascareta homologada es podria aconseguir fins a 5 mascaretes addicionals.

SEQR: Tecnologia per deixar un rastre digital segur per aplicacions sanitàries

B. Alorda-Ladaria, C. Carmona, J. Ballester, F. Mas
tomeu.alorda@uib.cat, +34 971 259941

SHARE&TECHNOLOGIES

IdISBa Institut d'Investigació Sanitària Illes Balears

Universitat de les Illes Balears

Problemàtica i objectius del treball

Eines de gestió recomanades per la Comissió Europea

Quina tecnologia podria contribuir al rastreig de contactes?
- Respectant la privacitat
- Respectant la LOPD
- Sense requerir contacte de superfícies
- Assegurant informació certa
- Amb infraestructura mínima o inexistent

Com transferir informació sanitària acreditada per un sistema sanitària extern a les Illes Balears?
- Transferència d'informació sanitària protegida
- Amb mínima infraestructura tecnològica

E-QR

- Permet acreditar informació en mobilitat
- Màxima informació reduint contagi durant la validació
- Manté la privacitat i autenticació de les dades
- Manté registre d'evidències de mobilitat pel rastreig de contactes

Descripció de la tecnologia

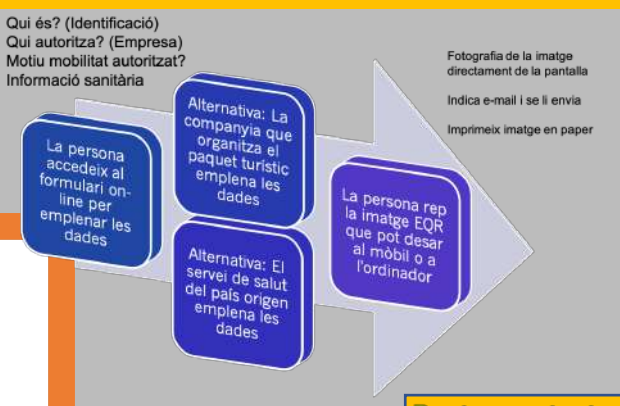

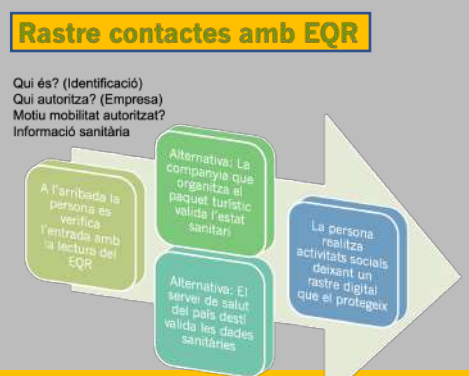

Disseny de protocols basats en la tecnologia EQR

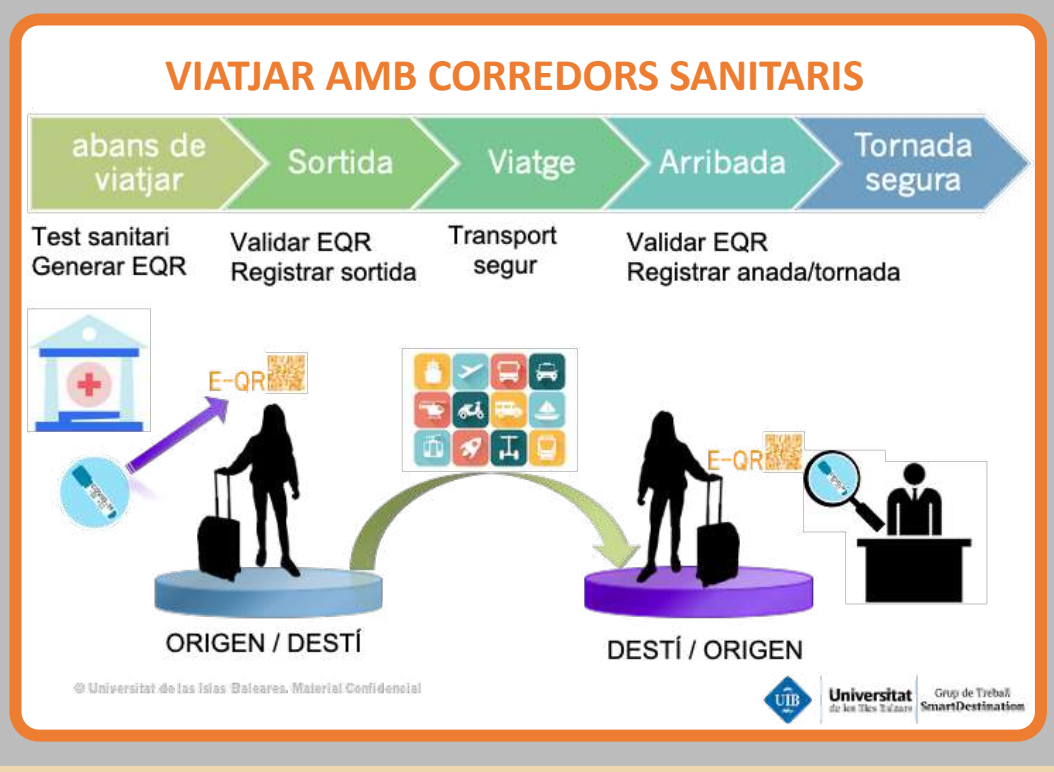

Epistatic Gene Pairs in Colon Cancer

Jairo Rocha[1], **Jaume Sastre**[1], **Emilia Amengual-Cladera**[2], **Victor Asensio**[2], **Damià Heine-Suñer**[2], **Emidio Capriotti**[3]

[1] Computational Biology and Bioinformatics Group (BIOCOM), University of the Balearic Islands
[2]Health Research Institute of the Balearic Islands (Idisba), Majorca, Palma, Spain
[3]Department of Pharmacy and Biotechnology (FaBiT), University of Bologna (Unibo), Bologna, Italy

Objective

To detect pairs of mutated genes in which the effect of the interaction between both mutations is significantly related to tumor/normal tissue while the effect of individual mutations is not significantly associated to the tumor/normal tissue. In other words, we aim to detect pairs of genes that have subjects where both genes mutated/not-mutated are significantly related to the tumor/normal tissue but each of the mutated genes by itself is not related to the tumor.

Background

Several methods have been used to detect individual driver mutations, which give a selective advantage to the cancerous cells and drive the onset of the disease from passenger mutations.

Other approaches try to find subnetworks of mutated genes in existing or known interaction networks that are correlated with the tumor [1].

We have analyzed paired mutational events in Colon Adenocarcinoma to detect pairs of genes frequently mutated in tumor samples potentially associated to the insurgence and progression of the disease. The relationship found may be new with respect to the known interaction networks.

Methods

We have $N = 422$ subjects with two exomes per subject:

- normal tissue sample, and
- tumor tissue sample.

Preprocessing

- There are $N = 422$ subjects in the TCGA from the Broad Institute.
- Synonymous SNPs are not considered.
- Variants mutated in normal but not in tumor tissues are not considered.
- Mutations with fewer than 10 reads of support are not considered (DP $\geq$ 10).
- To avoid genotyping errors, mutations with a ratio of reads supporting the alternate allele reads to total reads (AD/DP) inferior to 5% are not considered.
- The Minor Allele Frequency (MAF) of a variant must be below 70%.
- The number of subjects with a mutation in normal tissue should not be too high with respect to the MAF: the percentage of the 422 subjects that have a mutation in normal tissue should not exceed 0.5% + 1.25 $\times$ MAF.
- The number of subjects mutated in a gene tumor must be above 5% to be considered.
- Pseudogenes and olfatory genes are eliminated.

Statistical Association

Let be the binary variables:

- g_1: the gene 1 is mutated or not.
- g_2: the gene 2 is mutated or not.
- T: the sample is from normal or tumor tissue.

Decision on epistatic gene pair (g_1, g_2) using logistic regression:

- there is no association of $T \sim g_1$,
- there is no association of $T \sim g_2$, and
- the association $T \sim g_1 + g_2 + g_1 : g_2$ is significantly better than $T \sim g_1 + g_2$.

BOOST [2] performs efficiently the logistic regressions.

Results

- The number of genes considered after filtering is 14,661.
- There are 11,455 genes that are individually associated to the tumor, leaving 3,206 genes.
- All gene pairs are calculated for a total of 5,137,615 pairs.
- The Benjamini-Hochberg procedure with a false discovery rate q of 0.1 is applied.
- The pair passing the false discovery control is **KRTAP15-1 and KRTAP13-4** with a p-value of 1.2×10^{-8}.
- They are located in chromosome 21, nearby each other, 10,000 bases apart.
- It is calculated from the annotated VCF files in less than half an hour with 16 processors at 2.6GHz with programs in C, Python and R.

Biological Information

In the Genecards server [3], the descriptions that appear are:

KRTAP13-4: Diseases associated with KRTAP13-4 include **Atypical Neurofibroma**. Among its related pathways are Developmental Biology and Keratinization.

KRTAP15-1: Do not have diseases associated to it.

In Intogen [4], none of the two genes appear as tumor cancer drivers. This means that the models of Intogen do not individually associate these genes with any type of tumor.

In COSMIC [5] (Catalogue of Somatic Mutations in Cancer), the two genes do appear, so these genes were mutated in some subjects with cancer.

In STRING [6], the proteins KRTAP15-1 and KRTAP13-4 have no interaction not even at the low confidence level and also there is not a common protein between the neighbors of the two proteins at a low confidence level. Therefore, the proteins have not known previous relationship.

The two pairs of sites cited in [7] are in different chromosomes of ours (Chr 12 and 20).

Descriptive Statistics

Since a gene is considered mutated if any site in it is mutated, lots of genes are mutated in more than 100 subjects, out of 422 subjects.

The next figure shows that most subjects have less than 300 genes that are mutated only in tumor but not in normal tissue. Very few subjects have more than 800 genes mutated only in tumor. These values show the level of genetic degradation in tumor tissues.

Genetic degradation of tumor tissue. In this histogram of the frequency of subjects for each number of genes that are mutated only in tumor, we can see that there are around 170 subjects each of which has between 100 and 200 genes mutated only in tumor. Most subjects have less than 300 genes that are mutated only in tumor:

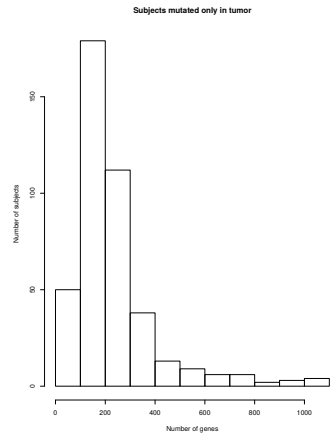

In the next figure we can see that there are few genes that are mutated only in tumor in more than 100 subjects and candidate for a single relationship with tumor. Most of these are discarded for the epistatic analysis.

Histogram of the frequency of genes mutated only in tumor tissue for each number of subjects. Very few genes are mutated in more than 100 subjects each: Most of these genes can be associated individually with the tumor appereance and are not reported in the epistatic analysis:

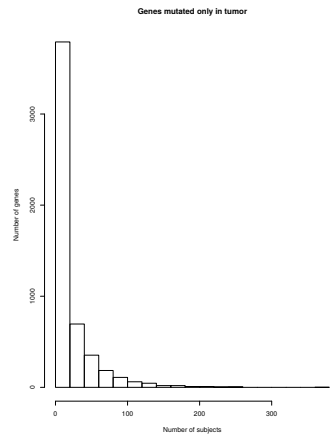

Conclusions

- We have a simple and fast procedure to detect epistatic mutation gene pairs related to tumor tissue without using previous known networks.
- It suggests a pair of gene whose mutation relationships could be investigated: **KRTAP15-1 and KRTAP13-4**.
- All the programs and data generated are available in *https://bass.uib.es/ jairo/epistasis*.

References

[1] T. Hansen and F. Vandin. Finding mutated subnetworks associated with survival time in cancer. In *RECOMB*, 2016.

[2] Xiang Wan, Can Yang, Qiang Yang, Hong Xue, Xiaodan Fan, Nelson L.S. Tang, and Weichuan Yu. Boost: A fast approach to detecting gene-gene interactions in genome-wide case-control studies. *The American Journal of Human Genetics*, (87):325–340, September 2010.

[3] G Stelzer et al. The genecards suite: From gene data mining to disease genome sequence analysis. *Current Protocols in Bioinformatic*, 54(1), 2016.

[4] A Gonzalez-Perez et al. Intogen-mutations identifies cancer nature methods. *Nature Methods*, 2013.

[5] J. Tate et al. COSMIC: the Catalogue Of Somatic Mutations In Cancer. *Nucleic Acids Research*, 47(D1):D941–D947, 10 2018.

[6] D. Szklarczyk et al. String v11: protein-protein association networks with increased coverage, supporting functional discovery in genome-wide experimental datasets. *Nucleic Acids Res*, 47, 2019.

[7] Shuo Jiao et al. Genome-wide search for gene-gene interactions in colorectal cancer. *PLoS ONE*, 7(12), 2012.

Acknowledgements

This research was partially supported by the Spanish Ministry of Science, Innovation and Universities and the European Regional Development Fund through the project PGC2018-096956-B-C43 (FEDER/ MICINN/AEI). Also, it has been funded by the projects PI13/02778 and PI18/00847 from Carlos III Health Institute (ISCIII) and by the grant 423/C/2015 from Fundació La Marató TV3.

Contact Information

- mailto: jairo@uib.es